Int J Adv Manuf Technol (2006) 29: 678–687
DOI 10.1007/s00170-005-2571-7

ORIGINAL ARTICLE

Kuen Ming Shu · Hung Rung Shih · G.C. Tu

Electrical discharge abrasive drilling of hard materials using a metal matrix composite electrode

Received: 22 March 2004 / Accepted: 15 January 2005 / Published online: 16 November 2005

Abstract The main object of the present work was to develop an electrical discharge abrasive drilling (EDAD) methodology to remove the re-solidified layer through the grinding induced by a metal matrix composite electrode prior to the re-solidification of molten material. A metal matrix composite (Cu/SiC_p) electrode, with an electroless pretreatment of Cu coating on SiC_p to enhance bonding status between Cu and SiC_p, was made with a rotating device and this was employed to study the EDAD technology. The machinability of the mold steel HPM50 and tungsten carbide P20 was investigated by the combined technologies of EDAD. The machined surfaces of these materials were examined by scanning electron microscopy (SEM) and their surface roughness measured by a profilemeter. From the experimental results, it was found that the EDAD machining efficiency was three to seven times than that of normal EDM operation for mold steel. However, the efficiency improvement is hardly detectable for tungsten carbide. In addition, the surface roughness of both materials could be improved in comparison with that achieved after EDM.

Keywords Cu/SiC_p composite · Electrical discharge abrasive drilling · Material removal rate · Surface roughness

1 Introduction

Electrical discharge machining (EDM) has been shown to be a versatile method for machining difficult-to-work material including heated-treated steels, tungsten carbides and various conductive ceramics [1–3]. However, low machining efficiency is one of the main EDM disadvantages. At present, many efficacious hybrid machining technique are employed to enhance the material removal rate (MRR) and/or surface roughness in EDM. Electrochemical discharge machining (ECDM) is a hybrid technology that incorporates ECM and EDM [4], ten times of MRR greater than that of conventional grinding for materials harder than HRc 60 can be obtained by this method [5]. Ultrasonic machining (USM) combined with EDM has been found to increase the MRR in machining hard materials like titanium alloy, tungsten carbide, titanium boride, etc [6–9].

The concept of combining EDM and diamond grinding for machining electrically conducting hard materials originated in the former USSR [10–12]. The process termed electrical discharge diamond grinding (EDDG) utilizes a metal bonded diamond-grinding wheel and subjects the work to the simultaneous influence of diamond grains and electrical sparks which cause abrasion and surface melting respectively.

Electro discharge dressing is a new method for dressing the diamond wheel that was glazed by intense wear attritions when grinding hard material. A maximum protrusion height close to 60% of the diamond grain size is achieved by this method [13]. In EDDG, it represents continuous in-process dressing of the grinding wheel, as material is eroded from the electrode as well. This obviates the need to interrupt machining for dressing the wheel. However, the EDDG can't be popularized because of the high loss of diamond wheel material and the production cost.

When the current flow ceases in EDM, a violent collapse of the plasma channel and vapor bubble causes superheated molten liquids on both the workpiece and electrode surfaces to explode into the gap, and the dielectric liquid solidifies the molten material immediately. However, the majority of the molten material cannot be removed because of its surface tension and bonding status between liquid and solid. The molten material remaining on the workpiece surface is cooled by the dielectric liquid, forming the recasted zone, and hence creates crater, ridge, and protrusion morphologies as observed on the EDMed surfaces [14].

K.M. Shu (✉) · H.R. Shih
Department of Mechanical Manufacturing Engineering,
National Formosa University,
Hu-wei, Yunlin, Taiwan, R.O.C.
E-mail: kmshu@sunws.nfu.edu.tw
Tel.: +886-5-6315327
Fax: +886-5-6315310

G.C. Tu
Department of Materials Science and Engineering,
National Chiao Tung University,
Hsinchu, Taiwan, R.O.C.

The main object of the present work was to develop an electrical discharge machining and grinding (EDAD) methodology to remove the protrusion through the grinding induced by a metal matrix composite electrode prior to the protrusion's solidification. To carry out the EDAD operation, there is clearly a need to have a high conductivity metal matrix composite electrode with anti-wear abrasive particles. Methods for fabricating metal based composite materials include melting and casting, co-precipitation, internal oxidation, and powder metallurgy [15]. Owing to the poor dispersion between metal and reinforcements, the melting and casting methods are impractical. The methods of co-precipitation and internal oxidation are not suitable for mass production; therefore, the powder metallurgy method, being capable of mass production, is the preferred choice in fabricating the composite electrode for the purpose of EDAD. For enhancing the bonding status between matrix and reinforcement of composite electrode, electroless copper plating on reinforcement surface is adopted in this research.

2 Experimental procedure

Metal matrix composites can be placed into three categories – particulate, fiber, and laminar – based on the shapes of the reinforced materials. The particulate composites contain large amounts of coarse particles that do not effectively block slip. SiC_p was selected as the reinforcement in this experiment for its superior mechanical properties of high hardness, high anti-wear stiffness during the grinding operation, high electrical conductivity to comply with the international annealed copper standard (IACS) electrode standard, and high thermal conductivity to obtain higher thermal shock resistance. Copper was selected as the matrix material for its high electric conductivity. The above-mentioned properties are all necessary for the EDAD electrode application.

The workpieces used in this study are P20 (Mitsubishi Co.) tungsten carbide and HPM 50 (Hitachi Co.) mold steel with a 4 mm hole through the center. The hole is created to ensure that the whole workpiece facing the electrode of 8 mm diameter is undergoing EDAD operation. The chemical compositions of the workpieces are shown in Table 1 and Table 2, respectively. Fig. 1a shows the microstructure of P20 after etching in Murakami's reagent (10 g $K_3Fe(CN)_6$, 10 g KOH, and 100 ml water) for 10 s; the etching outlines the carbide grains and darkens them slightly, while the Co binder is unaffected. Figure 1b shows the microstructure of HPM 50 after etching in 2% nital (2%HNO_3, 98%C_2H_5OH) solution; the etching attacks both ferrite grain boundaries (dark line) and the ferrite-cementite spheroid phase within grain. Not all the ferrite grain boundaries are clearly etched because of the orientation sensitivity of nital.

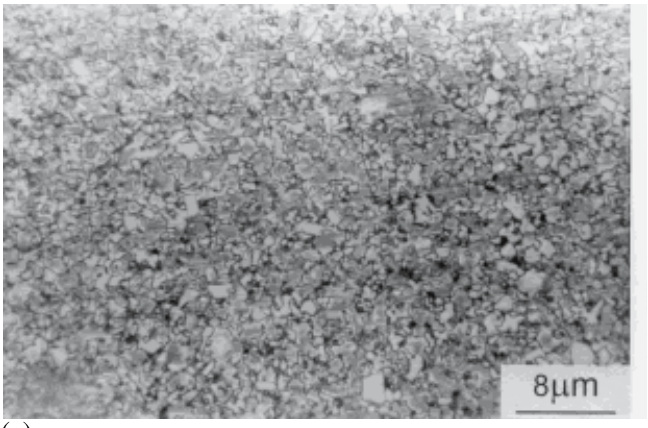

(a)

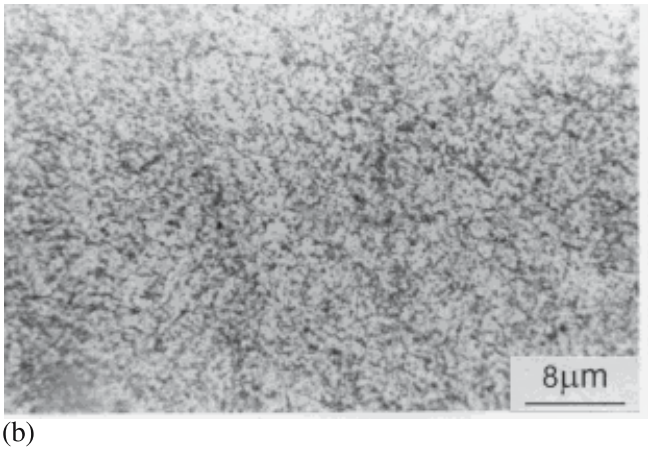

(b)

Fig. 1a,b. Micrographs of the mold material: **a** P20 WC and **b** HPM 50 mold steel

The EDAD processes were performed using a charm CM240C die-sinking machine. Table 3 lists the correlated parametric values or ranges adopted in this study.

The experimental set up of the EDAD process is schematically shown in Fig. 2. One of the primary objectives was to study the effect of electrode rotation. Therefore, a rotating facility was developed to allow the electrode to rotate at 0–2500 rpm. The electrode was rotated and sunk simultaneously to machine the

Table 1. The chemical composition of P20 tungsten carbide

Element	WC	TiC + TaC	Co
Wt.%	76	14	10

Table 2. The chemical composition of HPM50 mirror mold steel

Element	C	Si	Mn	Ni	Al	Cu	Mo	Fe
Wt.%	0.05-0.18	0.15-1.0	1.0-2.0	2.5-3.5	0.5-1.5	0.7-1.5	0.1-0.4	bal

Table 3. Design scheme of experimental parameters for EDAD

Electrical discharge machining and grinding conditions	
Work condition	Description
Workpiece	P20 WC and HPM 50 mirror mold steel
Electrode	Cu/SiC_p composite, ϕ 8 mm
Polarity (electrode)	Negative
Peak current (I_p)	1–5 A
Pulse duration (τ_{on})	125 μs
Pulse off time (τ_{off})	125 μs
Duty factor	0.5
Rotating speed (s)	$0 \sim 2500$ rpm
Dielectric fluid	CASTROL SPE oil. Flushing pressure 2 kg/cm^2

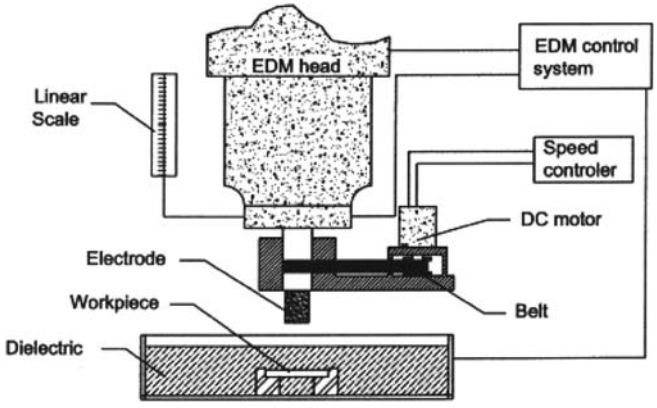

Fig. 2. Schematic experimental setup for EDAD process

workpiece. When the EDAD operation was introduced, as shown in Fig. 3, the protruded SiC_p mounted on the rotating electrode removed additionally the unsolidified protrusion by grinding it away. Since only the protruded SiC_p grains are in contact with the workpiece, a high normal force would cause indentation on the workpiece surface and the transverse movement of the electrode would cause grooves. Transverse movement would also let SiC_p grains be pulled out of the electrode if it were poorly mounted on the copper matrix, and this would result in the loss of both electrode material and grinding function. Although the maximum protrusion height, close to 60% of the grain size, can be achieved, approximately 30% of the grain size protrusion height was suggested [16] and employed in this paper. In Fig. 4, it can be seen that the SiC_p grains protrude from the copper matrix, and

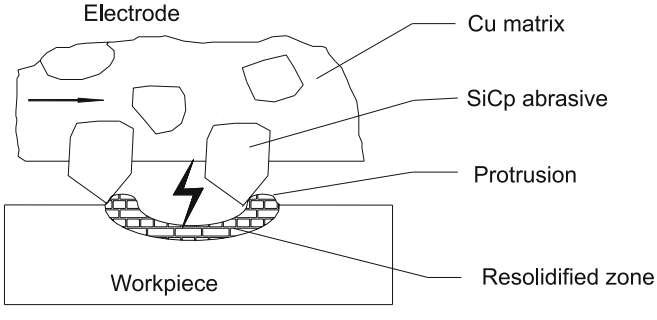

Fig. 3. Schematic representation of EDAD

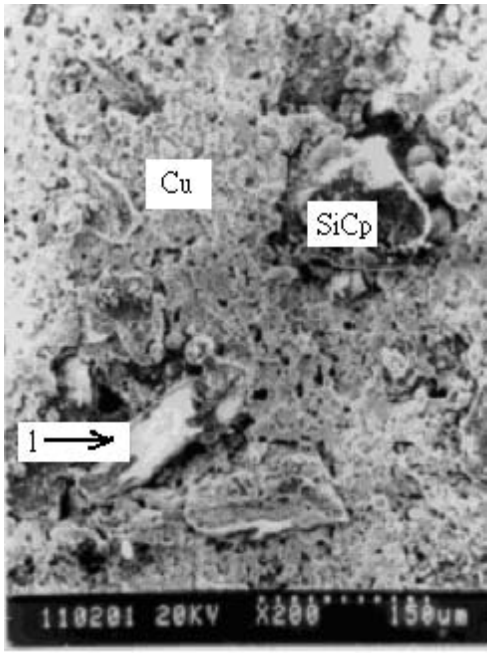

Fig. 4. The morphology of SiCp grains protruding from the copper matrix after EDAD process: (1) grinding trace on SiC_p, (2) Cu matrix, (3) SiC_p

the white grinding trace can be observed on the outmost portion of SiC_p after the grinding function was brought into effect.

The tool, Cu/SiC_p composite electrode, was of a cylindrical and flat-ended shape with a diameter of 8 mm and fabricated by the powder metallurgy method. The copper powder was of dendritic shape with a particle size range of 20–40 μm; the SiC_p powder, of an irregular polygonal shape with sharp angles and with 3, 63, 150, and 250 μm mean sizes, was used for reinforcement.

In order to obtain optimal bonding between the SiC_p and Cu matrix through a completely continuous copper film on SiC_p, electroless copper plating steps were applied.

The microstructure and fracture surfaces of composites are observed by optical microscope (OM) and scanning electron microscope (SEM). Uniaxial tensile testing with a constant crosshead speed of 1.0 mm/min was carried out on a instron testing machine at room temperature; specimens were machined according to ASTM E8 stand.

Copper powders with 0 and 20 wt.% SiC_p were mixed well and cold formed by pressing at 450 MPa pressure. A series of compacts were heated to 800 °C for 8 h in nitrogen. The working surface of sintered compact was etched by HNO_3 before the EDAD operation in order to create many qualified protrusions to physically interact with the workpiece. The dielectric fluid used was CASTROL SPE oil having a hydrocarbon base with a kinematic viscosity of 2.08 cst at 40 °C.

The front gap width between electrode and workpiece was measured as follows:

1. The electrode attached on the machine head was moved to contact with the workpiece before EDM was ignited and the dial gage on the EDM machine head was set at zero.

2. Raised the electrode, set the working current, then ignited EDM starting switch, the electrode would be moved toward the workpiece by servo mechanism.
3. The value showed on dial gage, when first series of spark ignited between the electrode and workpiece, gave the front gap width at the set working current.

3 Results and discussion

3.1 Discharge current effect in EDM

The main objective of EDAD of mold material is to generate a front spark gap between the electrode and workpiece leading grinding function occured precisely. Therefore, it was essential to determine the relationship of gap width to working current. The machining parameters such as the discharge current, breakdown voltage, pulse duration, dielectric strength, and electrode polarity have obvious effects on EDM performance. For the sake of simplification, only the discharge current factor was selected to change the front spark gap width, which is the most important factor for EDAD, as will be discussed in Sect. 3.4. Figure 5 shows the effect of varying discharge current on the front spark gap width with an electrolytic copper electrode containing 0 wt.% SiC_p. The results indicate that, whether using WC or HPM 50, the front gap width increases as the current increases, and there is little gap difference between the two materials.

Material removal rate is one of the important parameters for evaluating the EDM machining performance for a particular working setup. This rate depends on a large number of properties of the workpiece material, including its melting point, thermal conductivity, and latent heat. It is also influenced by the properties of the electrodes, and by geometric factors such as the shape and dimensions of the electrode and workpiece. Figure 5 also shows the variation of working current vs. material removal rate. The results also indicate that the MRRs of P20 WC and HPM 50 increase as the current increases.

3.2 Effect of electroless copper plating on electrode strength

Good bonding status between SiC_p and copper can prevent the SiC_p from peeling off the copper matrix when the grinding function is introduced in the EDAD operation. Through the electroless plating process, a copper film can be plated on a SiC_p surface fully and this copper film will diffuse with the copper matrix during the sintering process. Figure 6 shows the variation of tensile strength vs. SiC_p size, demonstrating that the tensile strength of composites using uncoated SiC_p is lower than that of composites with electroless copper plated SiC_p. SEM micrographs of the fracture surface of the composite with 3 μm, 20wt.% non-coated SiC_p are shown in Fig. 7a, in which arrow 1 indicates the decohesion of the SiC_p/Cu interface, and arrow 2 indicates SiC_p cracked by pressing or tensile test; all SiC_ps show relatively flat surfaces of row SiC_p powder shape, and these observations depict the poor bonding status for sintered Cu/SiC_p without electroless Cu plating pretreatment. The fracture surface of the composite with 3 μm, 20 wt.% coated SiC_p is shown in Fig. 7b, in which arrow 1 indicates SiC_p at the dimple bottom with the appearance of a covering of copper film, and arrows 2 and 3 indicate good bonding status between Cu and SiC_p, the copper film on the SiC_p surface is still observed on the fracture surface. In Fig. 7a, the fracture surface shows the presence of decohesion at the SiC_p/Cu interface. However, the occurrence of the SiC_p fracture is observed in Fig. 7b, and this indicates that there was a load transfer from the matrix to the SiC_p.

3.3 Observation of the electrical discharge machining and grinding surface

The EDMed surfaces of HPM 50 and P20 using row copper rod, i.e., 0 wt.% SiC_p, as an electrode are shown in Fig. 8. It generally

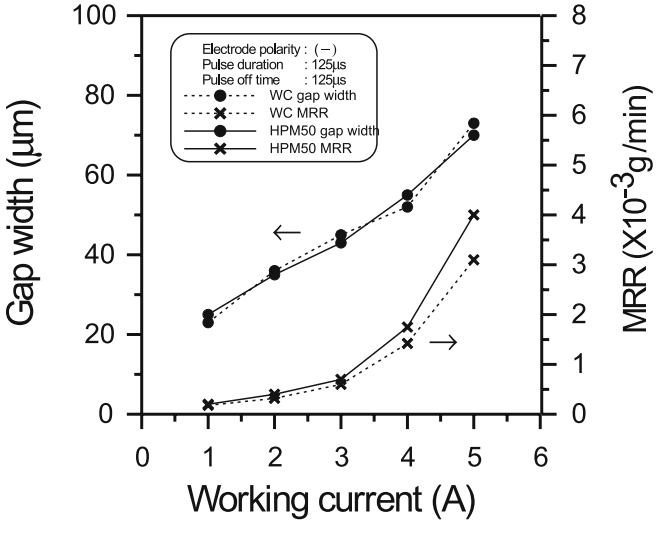

Fig. 5. Effects of working current on gap width and MRR using a copper electrode for WC and HPM50 as work materials

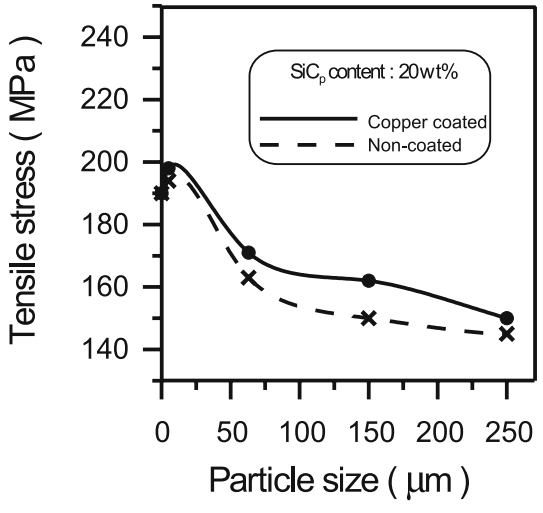

Fig. 6. Effect of particle size on the tensile stress of sintered Cu/SiC composite

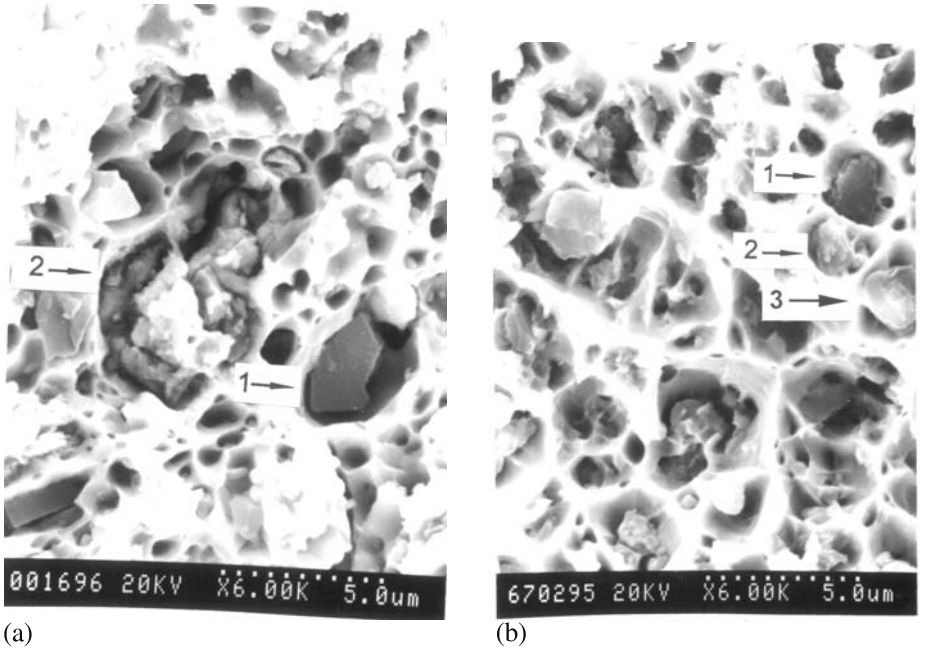

(a) (b)

Fig. 7a,b. SEM micrographs of the fracture surface of: **a** non-coated electrode, **b** copper coated electrode

has a complex appearance covered by shallow craters, spherical particles, and pockmarks formed by entrapped gases escaping from the redeposit material on HPM 50 (Fig. 8a). A number of evenly distributed network grain boundaries are identified on the P20 workpiece (Fig. 8b), and pinholes can also be observed on the grain surface, apparently caused by gas bubbles expelled from the molten material during solidification. Typical surface structures of HPM 50 mold steel surface machined by EDAD are shown in Fig. 9. In Fig. 9a, with a 63 μm SiC_p electrode and 2A working current, the estimated SiC_p protrusion value is 19 μm (30% of the SiC_p size) and the average front spark gap is 35 μm (obtained from Fig. 5). The former is much smaller than the latter. It seems that the electrical discharge grinding function has little effect on the workpiece surface, for only some shallow grinding traces were observed on the bigger spherical particles surface or higher protrusion of the workpiece.

With a 250 μm SiC_p electrode and 2A working current, as shown in Fig. 9b, the estimated SiC_p protrusion is 75 μm and the front spark gap between the matrix and workpiece is 36 μm approximately. The SiC_p protrusion passes through the resolidified

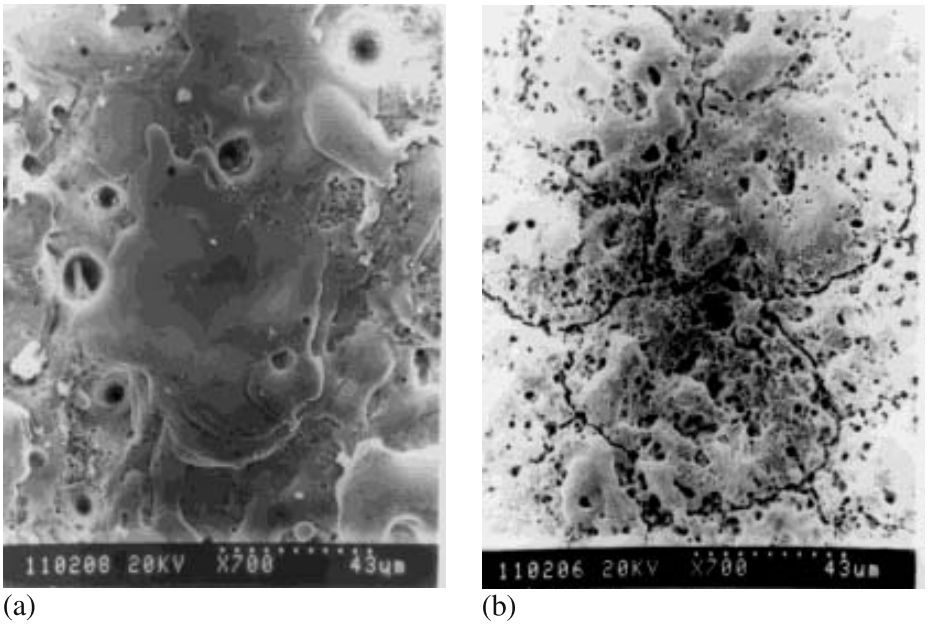

(a) (b)

Fig. 8a,b. The typical morphology of an EDMed surface using row copper electrode: **a** HPM50, **b** P20

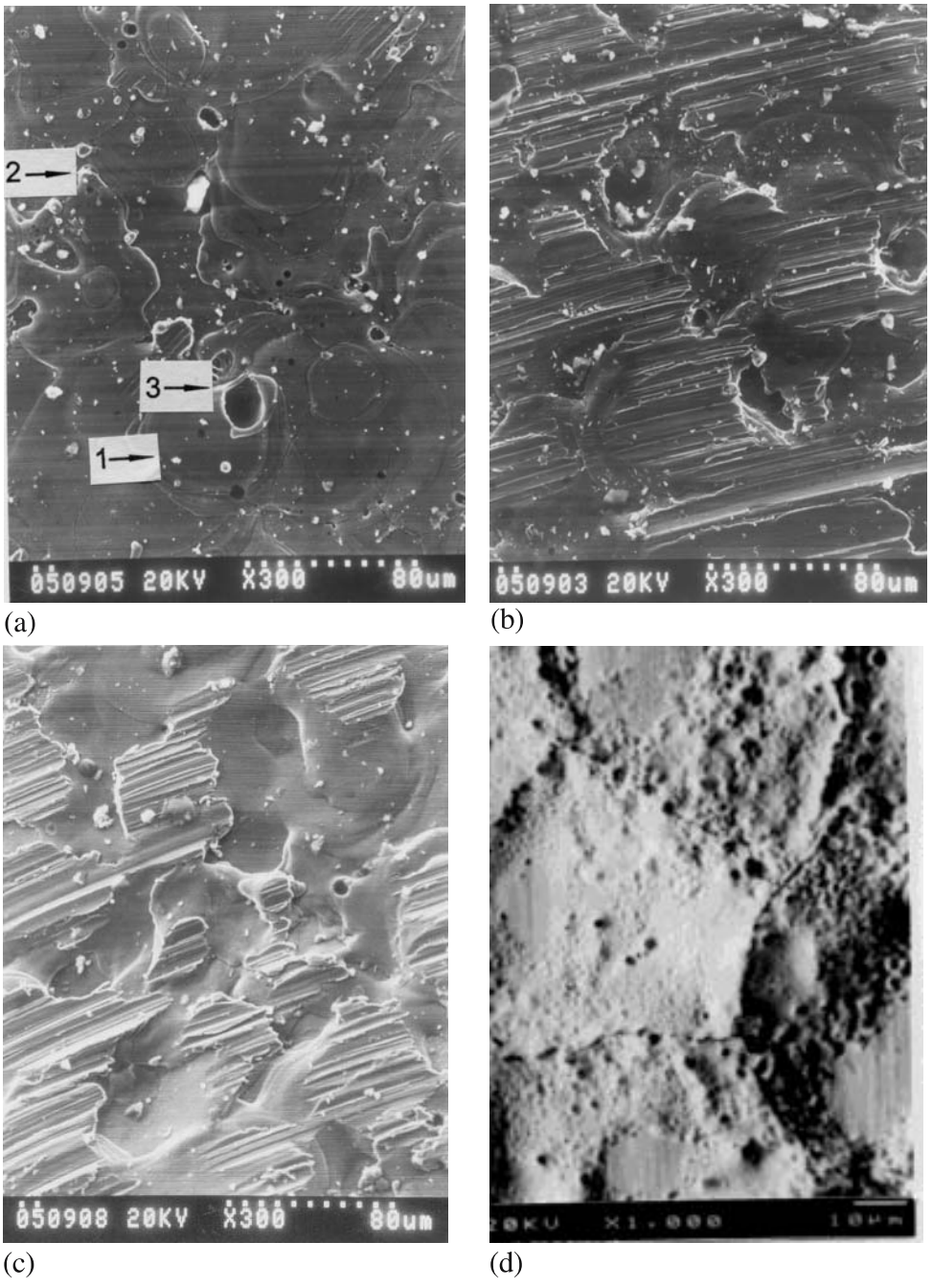

Fig. 9a–d. SEM micrograph showing surface morphology of EDADed that with composite electrode of various SiC_p sizes at 2250 rpm rotating speed, 125 ms pulse-on time and 2 A current setting: **a** HPM 50, 63 μm SiC_p, 1 is crater, 2 is spherical particle, 3 is pock mark. **b** HPM 50, 250 μm SiC_p, **c** HPM 50, 150 μm SiC_p, **d** P20, 150 μm SiC_p

zone and penetrates into the heat-affected zone, or possibly even deep into the matrix. Under this EDAD condition, the material removal rate is attributed mainly to the grinding mechanism. Evident proof of the dominant grinding effect can be found from the grinding marks covering the whole EDADed surface, except for some deeper craters caused by the EDM mechanism.

When SiC_p size and working current were optimally selected with a 150 μm SiC_p electrode and 2A working current, only the protrusion around the spark crater was ground away from the matrix, as shown in Fig. 9c. The total material removal rate under this EDAD condition is attributed to both the EDM process and the protrusion grinding process.

In Fig. 9d, when 150 μm SiC_p size and 2A working current were selected to EDAD P20 WC/Co, the dominant grinding mechanisms were still unclarified since both WC and SiC_p possess a high melting point (SiC_p: 2600 °C, WC: 2720 °C) and high room temperature microhardness (Knoop, SiC_p: 2200–3000 kg mm^{-2}, WC: 1700–2400 kg mm^{-2}) [17]. From the observation of the shallower grinding mark on the EDADed P20 surface, it seems that the WC/Co recast layer can still be ground

by SiC_p possibly due to the fact that its hardness is substantially higher than that of WC. However, the heat affected zone and matrix of the working piece are too hard to be attacked by Cu/SiC_p drilling.

Figure 10 shows the optical micrograph of the cross-section taken from HPM50 specimens after the EDAD operation, in which three layers are observed: resolidified layer, heat affected layer, and matrix. When etched with a dilute nitric acid solution, the outmost layer (called white layer) in these specimens remained bright and featureless, i.e., they were nonetchable. This white layer was formed when the outermost molten material was quenched at an extremely high rate by flushes of the dielectric. The optical micrograph of Fig. 10a shows the white layer of the EDADed surface with a 63 μm SiC_p electrode, and both pock marks and microcracks are observed on this layer and no grinding trace is observed in this figure. Figure 10b shows the white layer of specimens with optimum SiC_p content and electrode-rotating speed, a thin white layer after grinding action is observed, and the ungrounded white layer has the same thickness as that of the white layer in Fig. 10a. Using an electrode with a larger SiC_p size, the white layer is pricked, and the heat affect zone is ground by SiC_p directly, and the results are shown clearly in Fig. 10c.

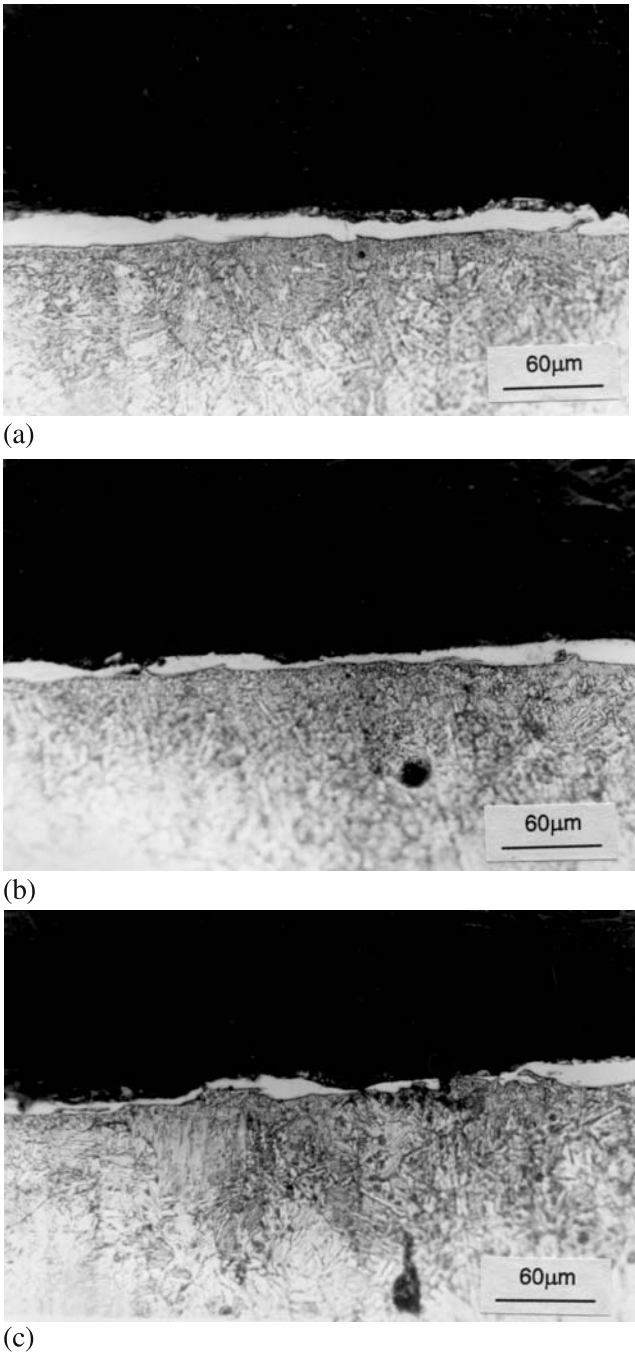

Fig. 10a–c. Optical micrograph showing the thickness of the white layer of HPM 50 after EDADed with various SiC_p sizes electrode at 2250 rpm rotating speed, 2 A current setting, 125 μs pulse-on time: **a** 63 μm SiC_p, **b** 150 μm SiC_p, **c** 250 μm SiC_p

To understand the mechanism of particle size effect on EDAD, it is necessary to examine the relationship between the gap width between the workpiece and electrode, the thickness of the recasted zone and the SiC_p size. A schematic illustration of these relationships is presented in Fig. 11, where HPM 50 was adopted for consideration. The white layer thicknesses were measured at various points on different cross sections of the specimen EDADed at the selected current; the width was obtained by measuring the gap from the electrode top surface to the workpiece surface; the SiC_p grains' protrusion height was about 30% of the average SiC_p grain size. As can be seen from Fig. 11a, when the working current was set at 1 A, the

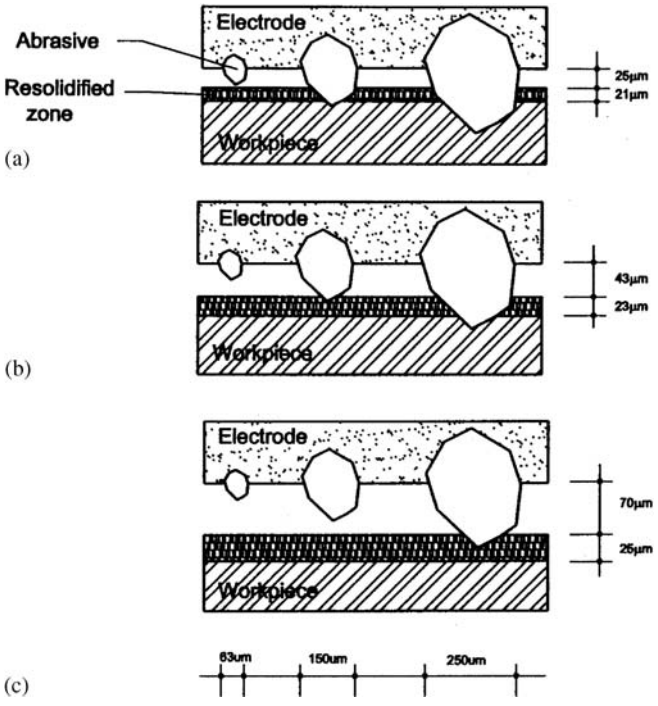

Fig. 11a–c. Schematic illustration of the relationships between particle size, gap width and thickness of recasted zone with various currents: **a** 1 A, **b** 3 A, **c** 5 A

gap width between the electrode and workpiece shown in Fig. 5 was 25 μm and the recasted zone was 21 μm. The protrusion of the electrode with 63 μm SiC_p was 19 μm, which was almost in contact with the recasted zone, and the grinding function had little effect on the workpiece surface. The MRR of EDAD were nearly the same as that of EDM, using copper as the electrode. The white layer was ground by the particle protrusion of the electrode with 150 μm SiC_p, and the matrix was ground by the particle protrusion of the electrode with 250 μm SiC_p. Gap width and recasted zone thickness increased with increasing working current. In Figs. 11b and c, when 3 A and 5 A current were set, the gap width was 43 μm and 70 μm, and the average recasted zone thickness was 23 μm and 25 μm respectively. Only at the particle protrusion of electrode contacts recasted zone can grinding action occur, i.e., the matrix would be ground at 3 A working current with a 250 μm SiC_p electrode and only the protrusion was ground when at 3 A working current with a 150 μm SiC_p electrode and 5 A working current with a 250 μm SiC_p electrode.

The appearance of the EDADed surface (Figs. 9b and c) depicts that the protrusion and the spherical particles, protruding from the workpiece surface, would be ground first by the protruded SiC_p. Undoubtedly, the surface roughness of the EDADed surface would therefore be finer than that of the EDMed surface. Figure 12 shows that the surface roughness of the HPM 50 EDADed surface using electrodes with 0 μm and 3 μm SiC_p is higher than that of the electrode with SiC_p sizes larger than 63 μm, and this is attributed to the electrode grinding function being introduced on the workpiece surface. In addition, the surface roughness of the EDADed HPM 50 surface using an electrode with 3 μm SiC_p is higher than that with 0 μm SiC_p, and this is possibly explained as follows: when at the same working current and working area, the electrode with 3 μm SiC_p can induce higher current density on a workpiece because some Cu is replaced by SiC_p, and this leads to the localized workpiece melting and vaporizing. Deeper craters and higher protrusions are thus induced and this results in higher surface roughness. When applying EDAD P20, the surface roughness increased as the SiC_p size of electrode varied from 0 μm to 3 μm, possibly

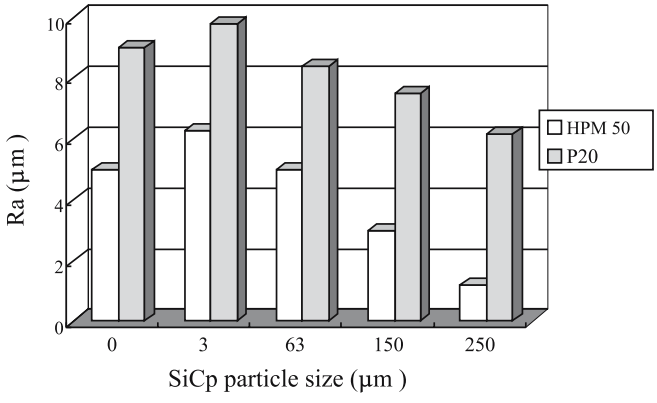

Fig. 12. The surface roughness of an EDADed surface at 2250 rpm rotation speed, 125 μs pulse-on time and 2A current setting

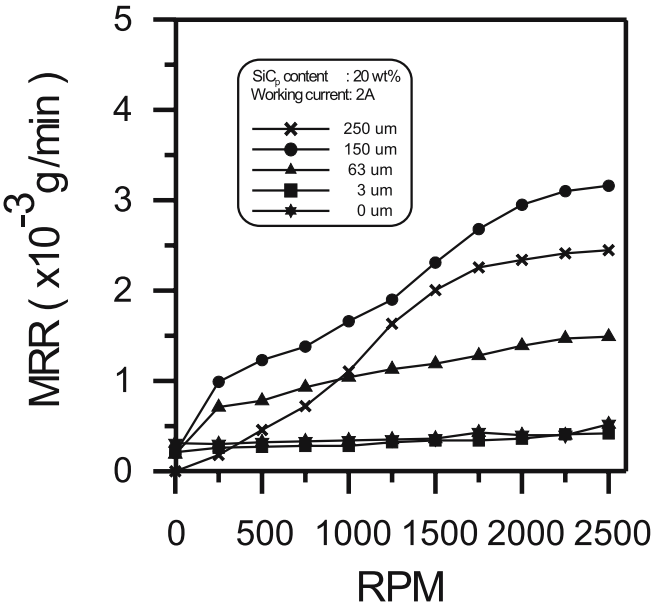

Fig. 13. The effect of electrode rotating speed on MRR of HPM 50 using electrodes with various SiC_p sizes

for the same reason as mentioned above. However, the slow decrease of surface roughness with SiC_p sizes increasing from 3 μm to 250 μm on EDAD P20 could be caused by the fact that the grinding action on WC/Co could not function as effectively as that on WC.

3.4 Effects of electrode rotating speed and working current on MRR

The results in Fig. 13, when HPM 50 is selected as the workpiece, show the effect of electrode rotating speed on MRR with various SiC_p size electrodes at 2 A working current. It demonstrates that all of the MRRs of EDAD, when using composite electrodes and at 0 RPM rotating speed, are lower than when using a pure copper electrode; the MRR of EDAD approached zero when the 250 μm SiC_p electrode was used. These phenomena may be explained as follows: when EDAD is performed with composite electrode, and the electrode and workpiece are moved to a very small gap by servomechanism, only the copper, which possesses low electrical resistance on the electrode front surface, can generate a spark. No sparks were induced from the SiC_p to the workpiece because of the high electrical resistance of the SiC_p. Consequently, the surface area occupied by Cu metal on the electrode front is the major factor in determining the MRRs by EDM while using the same machining parameters. As the SiC_p wt.% increases in the electrode, the area occupied by Cu on the electrode front would be lessened leading to a decreased sparking area and resulting in a lower MRR. For the electrode with 250 μm SiC_p, the SiC_p protrusions are larger than the spark gap, therefore no spark was generated between electrode and workpiece unless the protruded 250 μm SiC_p were crushed by moving the EDM machine head forward to form a smaller SiC_p protrusion and let a spark be generated. This is the reason why

the MRR of EDAD is near zero when using 250 μm SiC_p electrode at 0 RPM rotating speed.

When EDAD was performed with a copper electrode or 3 μm SiC_p electrode, the MRR retained a low value, i.e., 0.3×10^{-3} g/min in this experiment, despite the electrode rotating speed being gradually increased. This is attributed to the fact that no grinding action happened between the electrode and workpiece since nil SiC_p protrusion could grind the workpiece surface, or the SiC_p protrusions were too short to grind the workpiece surface. The MRRs under this machining condition were dominated by the EDM operation. In comparison with the MRR of the copper electrode, the larger SiC_p size (i.e., > 3 μm) electrodes exhibited far lower MRRs than did the copper electrode. It also can be observed that the MRR of EDAD with a 3 μm SiC_p electrode is slightly lower than that of the copper electrode. This phenomenon complies well with the EDAD mechanism.

When EDAD uses a 63 μm SiC_p electrode, the MRR of EDAD increases steadily as electrode rotating speed increases, since the grinding operation is introduced and only the top height of the EDM surface was ground away (as shown in Fig. 9). The MRR increment can be attributed to the fact that more material was being ground away by the SiC_p as the electrode-rotating speed increased. When EDAD uses a 150 μm SiC_p electrode, the MRR of EDAD also increases steadily from 0 to the 1250 RPM electrode rotating speed range. The MRR values are higher than that of a 63 μm SiC_p electrode, for more SiC_p protrusion enables the attacking of the resolidified layer. However, it is interesting to note that when the electrode rotating speed is over 1250 RPM, the MRR of EDAD increased dramatically and leveled off after 2250 RPM. This is attributed to the fact that under this high rotating speed condition the unsolidified layer had the capability (or the possibility) to encounter the protruded SiC_p and was ground away by SiC_p, leading to much higher MRR values.

When EDAD with a 250 μm SiC_p electrode was used, the MRR increased with the higher electrode rotating speed from 0 to 1000 RPM. In this stage, only the grinding function was performed, for the SiC_p protrusions were far greater than the spark gap. The MRR was attributed to the grinding action and increased with higher electrode rotating speed. However, in practice, the SiC_p protrusions would be pressed ahead and become smaller after crushing with the workpiece by the EDM machine head's servo movement; the smaller crushed SiC_p would grind the recasted zone. Consequently, the MRR increments are also observed from 1000 RPM to 1750 RPM. When the rotating speed exceeds 1750 RPM, the MRR increments tend to level off. The MRR of EDAD are still lower than that with 150 μm SiC_p electrode. From the above results, it is suggested that the EDAD process can be achieved only under optimum condition of choosing SiCp size, electrode speed and working current.

Figure 14 shows the specific value of MRR, i.e., the ratio of MRR (EDAD) /MRR (EDM), using various SiC_p size electrodes and working currents. When optimum machining parameters are selected (which in the present study are 2250 RPM electrode rotating speed, 2 A working current, and 150 μm SiC_p electrode), it was found that as high as seven times the normal EDM material removal rate could be achieved in EDAD operation. Allied with the expected finer surface roughness in EDAD than the EDM processes (as described in the last paragraph of Sect. 3.3), the EDAD appears a much better processing choice than EDM.

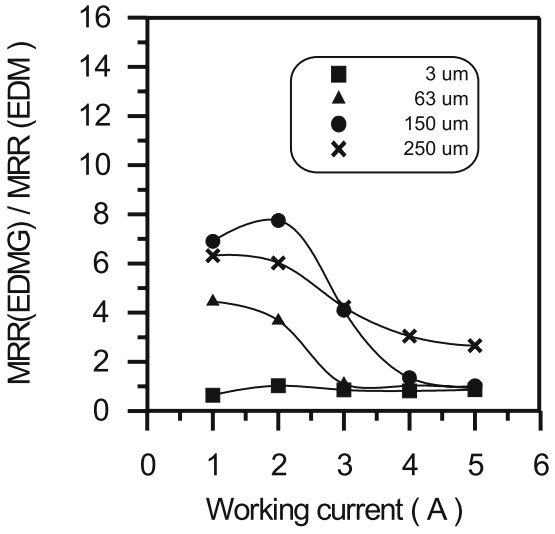

Fig. 14. The specific value of the MRR of EDM and EDAD of HPM 50 at different SiC_p and working currents with 2250rpm electrode rotating speed

4 Conclusions

The combined functions of electrical discharge abrasive drilling (EDAD) can be soundly realized by using an electrode rotating facility with well-bounded metal matrix composite electrode (Cu/SiC_p) made by the powder metallurgy method. The function mechanism is proposed and discussed. Higher material removal rate and lower surface roughness can be achieved when suitable electrode rotating speed, SiC_p size, and working current are chosen. Experimental results showed that when using HPM 50 mold steel as the workpiece, the EDAD machining efficiency was three to seven times that of normal EDM operation. The surface roughness of P20 and HPM50 could be improved in comparison with that achieved after EDM.

References

1. Llanes L, Idanez E, Martinez E, Casas B, Esteve J (2001) Influence of electrical discharge machining on the sliding contact response of cemented carbides. Int J Refract Metals Hard Mater 19:pp35-40
2. Khairy ABE (1990) Die-sinking by electrosion-dissolution machining. Ann CIRP 39(1):191–195
3. Trueman CS, Huddleston J (2000) Material removal by spalling during EDM of ceramics. J Eur Ceramic Soc 20:1629–1635
4. McGeough JA, De Silva A, Senbel HA, Lee SC, Wang JY (2001) Wheel dressing and discharge effects in electrochemical grinding of titanium alloy. Proc 13th ISEM CIRP 1:327–337
5. Benedict GF (1987) Non-traditional manufacturing processes. Dekker, New York
6. Lin YC, Yan BH, Chang YS (2000) Machining characteristics of titanium alloy using combination process of EDM with USM. J Mater Process Technol 104:171–177

7. Zhixin J, Jianhua Z, Xing A (1997) Study on a new kind of combined machining technology of ultrasonic machining and electrical discharge machining. Int J Mach Tools Manuf 37(2):193–199
8. Thoe TB, Aspinwall DK, Killey N (1999) Combined ultrasonic and electrical discharge machining of ceramic coated nickel alloy. 92(93):323–328
9. Wansheng Z, Zhenlong W, Shichun D, Guanxin C, Hongyu W (2002) Ultrasonic and electric discharge machining to deep and small hole on titanium alloy. J Mater Process Technol 120:101–108
10. Ya Grodzinskii E (1979) Grinding with electrical activation of the wheel surface. Mach Tooling 50:10–17
11. Vitlin VB (1981) Model of the electrocontact-abrasive cutting process. Sov Eng Res 1(5):88–98
12. Ya Grodzinskii E, Zubotava LS(1982) Electrochemical and electrical-discharge abrasive machining. Sov Eng Res 2(3):90–98
13. Wang X, Ying B, Liu W (1996) EDM dressing of fine grain super abrasive grinding wheel. J Mater Process Technol 62:299–302
14. Snoeys R, Van Dyck F (1972) Plsma channel diameter growth affects stock removal in EDM. Ann CIRP 21 (1):39–40
15. Matthews FL, Rawlings RD (1993) Composite materials: engineering and science. Chapman Hall, London
16. Koshy P, Jain VK, Lal GK (1996) Mechanism of material removal in electrical discharge diamond grinding. Int J Mach Tools Manuf 36(10):1173–1185
17. Sunniva RK (1989) ASM engineered materials reference book. ASM International, Metals Park, OH